Gait & Posture 113 (2024) 158–166

Contents lists available at ScienceDirect

Gait & Posture

journal homepage: www.elsevier.com/locate/gaitpost

ESMAC Best Paper Award 2023: Increased knee flexion in participants with cerebral palsy results in altered stresses at the distal femoral growth plate compared to a typically developing cohort

Willi Koller [a,b,c,*], Elias Wallnöfer [a,b], Jana Holder [d], Andreas Kranzl [e,g], Gabriel Mindler [f,g], Arnold Baca [a], Hans Kainz [a,b]

[a] Department of Sport and Human Movement Science, Centre for Sport Science and University Sports, University of Vienna, Vienna, Austria
[b] Neuromechanics Research Group, Centre for Sport Science and University Sports, University of Vienna, Vienna, Austria
[c] Vienna Doctoral School of Pharmaceutical, Nutritional and Sport Sciences, University of Vienna, Vienna, Austria
[d] Department of Sport and Exercise Science, University of Salzburg, Salzburg, Austria
[e] Laboratory for Gait and Human Movements, Orthopaedic Hospital Speising, Vienna, Austria
[f] Department of Pediatric Orthopaedics, Orthopaedic Hospital Speising, Vienna, Austria
[g] Vienna Bone and Growth Center, Vienna, Austria

ARTICLE INFO

Keywords:
Femoral bone growth
Finite element analysis
Osteogenic index
Distal growth plate
MRI-informed modeling
Semi-automated growth predictions

ABSTRACT

Introduction: Femoral deformities are highly prevalent in children with cerebral palsy (CP) and can have a severe impact on patients' gait abilities. While the mechanical stress regime within the distal femoral growth plate remains underexplored, understanding it is crucial given bone's adaptive response to mechanical stimuli. We quantified stresses at the distal femoral growth plate to deepen our understanding of the relationship between healthy and pathological gait patterns, internal loading, and femoral growth patterns.

Methods: This study included three-dimensional motion capture data and magnetic resonance images of 13 typically developing children and twelve participants with cerebral palsy. Employing a multi-scale mechano-biological approach, integrating musculoskeletal simulations and subject-specific finite element analysis, we investigated the orientation of the distal femoral growth plate and the stresses within it. Limbs of participants with CP were grouped depending on their knee flexion kinematics during stance phase as this potentially changes the stresses induced by knee and patellofemoral joint contact forces.

Results: Despite similar growth plate orientation across groups, significant differences were observed in the shape and distribution of growth values. Higher growth rates were noted in the anterior compartment in CP limbs with high knee flexion while CP limbs with normal knee flexion showed high similarity to the group of healthy participants.

Discussion: Results indicate that the knee flexion angle during the stance phase is of high relevance for typical bone growth at the distal femur. The evaluated growth rates reveal plausible results, as long-term promoted growth in the anterior compartment leads to anterior bending of the femur which was confirmed for the group with high knee flexion through analyses of the femoral geometry. The framework for these multi-scale simulations has been made accessible on GitHub, empowering peers to conduct similar mechanobiological studies. Advancing our understanding of femoral bone development could ultimately support clinical decision-making.

1. Introduction

Cerebral palsy (CP) is a neurological disorder where neuro-musculoskeletal abnormalities result in progressive disabilities in activities of daily living. Gait impairments lead to decreased mobility depending on the severity of the disease. Pathological bone deformations of the femur are common problems in this patient cohort and are often treated with corrective de-rotation or re-alignment

* Corresponding author at: Department of Sport and Human Movement Science, Centre for Sport Science and University Sports, University of Vienna, Vienna, Austria.
E-mail address: willi.koller@univie.ac.at (W. Koller).

https://doi.org/10.1016/j.gaitpost.2024.06.012
Received 9 December 2023; Received in revised form 21 May 2024; Accepted 17 June 2024
Available online 18 June 2024

osteotomies performed during multi-level surgeries [1]. It has been shown that bone adapts its shape and strength in response to mechanical loading [2–7]. A better understanding of the relationship between gait patterns, loading on the bones and bone growth could help inform early-stage interventions to avoid the development of femoral deformities.

Cross-sectional studies have shown that the femoral neck-shaft angle (NSA) and anteversion angle (AVA) decrease during growth in typically developing (TD) children. Children with CP often have increased NSA and AVA [8–10]. Pathological bony geometries alter moment arms of muscles [11] which can affect muscle recruitment strategy [12] and therefore bone loads [13] and growth. The stresses within the proximal femoral neck growth plate determine the development of the femoral geometry in terms of NSA and AVA. Multi-scale studies based on musculoskeletal (MSK) and finite element (FE) simulations have been used to estimate muscle forces, joint contact forces and stresses within the proximal femoral neck growth plate [14–20]. Summarized, these studies conclude that stresses within the growth plate are sensitive to the overall femoral geometry [19], the geometry of the growth plate itself [16] and the loading conditions [14,15,17–19].

Data from the individual's bony geometry and walking pattern are required to estimate bone loads and perform mechanobiological simulations. Bony geometry can be obtained from medical images, e.g. computer tomography or magnetic resonance imaging. Furthermore, the walking pattern of a person can be objectively quantified with the use of instrumented three-dimensional gait analysis. The loading on the bones, i.e., joint contact forces and muscle forces, during activities of daily living cannot be measured in-vivo but estimated based on the gait analysis data, i.e. marker trajectories and ground reaction forces, using MSK simulations [21–23]. Subject-specific personalization of the bony geometries in the MSK model has been shown to improve the agreement between measured and estimated joint contact forces [24,25]. Individualized FE models with a hexahedral mesh aligned with the growth plate are required to calculate growth plate stresses for the mechanobiological growth simulations but are time-consuming to create. Therefore, previous studies mainly analyzed a small number of individuals (1–4 participants) [14–19,26], which did not allow a generalization of the results, or used generic FE models [15,27]. We recently developed a tool to create the FE models for the mechanobiological simulations in a semi-automated method, which enabled us to analyze growth plate stresses within the femoral neck growth plate of the femur in a comparably large dataset of 50 femurs [20]. We showed that the variability of the growth plate stresses within the CP group is significantly larger compared to the TD group indicating pathological growth patterns in some of the CP participants [20].

Mechanical lower limb axis malalignments, e.g. varus/valgus deformities, are common in adults and children with and without neurological disorders, e.g. CP [28,29]. Growth at the distal femoral epiphyseal plate influences the mechanical lower limb axis and is often guided by the use of temporary hemiepiphysiodesis [30–32]. Hucke et al. [26] recently showed that the stresses induced by an hemiepiphysiodesis reduced the growth rate at the implanted region in three patients. Furthermore, the authors highlighted that the subject-specific loading based on the person's gait pattern and the subject-specific shape of the growth plate are important factors influencing the growth plate stresses. The femoral AVA and NSA was not personalized in their models, which is known to influence hip and knee joint contact forces [33] and therefore growth plate stresses. To the best of the authors' knowledge, no studies have quantified the stresses within the distal femoral growth plate in healthy children. Knowing typical growth plate stresses in healthy children is a prerequisite to gain a deeper understanding of the relationship between healthy and pathological gait patterns, internal loading and femoral growth.

The aim of the present study was to comprehensively analyze the stresses within the distal femoral growth plate in TD children and participants with CP. To achieve this aim, we enhanced our previously developed workflow and develop a tool to quantify subject-specific stresses at the distal femoral growth plate based on medical images and 3D motion capture data. Patients with CP have individual walking styles which can be classified into several patterns depending on the hip, knee and ankle kinematics [34]. Because knee kinematics influences knee joint contact forces [22] and stresses in the distal femoral growth plate, we divided the limbs of our CP participants in different groups depending on their knee kinematics. In addition to growth plate stresses, we compared the orientation of the growth plate between the CP groups and a group of TD participants. We hypothesized that 1) the orientation of the growth plates does not differ between TD children and participants with CP, 2) stresses at the distal growth plate differ between TD children and participants with CP due to different gait patterns, and 3) growth plate stresses differ between CP participants with different knee kinematics.

2. Materials and methods

The details regarding the materials and methods utilized in this study are briefly outlined in the main manuscript. For a more comprehensive understanding, a thorough methods section containing all details can be found in the supplementary material.

2.1. Data collection

Magnetic resonance images (MRI) and three-dimensional gait analysis data including marker trajectories and ground reaction forces of thirteen TD children (10 ± 2.2 years old, height: 144.5 ± 8.5 cm, mass: 36.8 ± 9.5 kg) and twelve participants diagnosed with CP (10.4 ± 3.8 years old, height: 133.6 ± 16.1 cm, mass: 30.1 ± 10.8 kg) with various walking patterns were analyzed for this study. Detailed information of participants with CP including Gross Motor Function Classification System (GMFCS), clinical diagnosis, age, sex, walking style and assigned group is presented in Table 1. All participants walked without walking aids and with a self-selected speed. Details of the data collection of the CP participants and three TD children are described by Kainz et al. [34]. The data of the remaining ten TD children was collected in the same manner, details are described in a previous publication [20].

2.2. MRI measurements, MSK and FE simulations

MRI scans were used to calculate femoral AVA and NSA [37]. The intercondylar distance, i.e. distance between the medial and lateral condyles of the femur, was quantified from the MRIs. MRI scans of the whole lower limbs were available in all CP and three TD participants, which enables us to additionally measure the tibial torsion [38] in these participants. These measurements were used to create subject-specific MSK models based on an OpenSim model [39], an alteration of the Rajagopal model [40] including the more complex knee joint of the Lerner model [24], which allows estimation of medial and lateral knees joint contact forces (KCF) as well as the patellofemoral joint contact force (PCF). To personalize the base model, the Torsion Tool [41] was used to modify the bony geometry to match each participant's NSA and AVA as well as tibial torsion, if MRI scans of the tibia were available. To fit the model to each participant's anthropometry, the pelvis, femur and tibia (if available) were scaled based on MRI measurements while the remaining body segments were scaled based on the location of surface markers [35]. Furthermore, the intercondylar distance was modified in the models to match each participant's value obtained from the MRI images [24]. Each participant's model and the corresponding gait analysis data were used to calculate joint angles, muscle forces and joint contact forces using inverse kinematics, static optimization by minimizing the sum of squared muscle activations and joint reaction load analyses with OpenSim 4.2, respectively [21,22].

Each femur was segmented using 3D Slicer [42] and divided into six parts representing different structural parts similar to previous studies

Table 1
Age, sex, clinical diagnoses, Gross Motor Function Classification Score (GMFCS), walking style based on visual inspection of marker data [36] and knee flexion classification of the participants with CP.

	Age	Sex	Diagnosis from clinicians	GMFCS	Walking style		Knee flexion group	
					Left	Right	Left	Right
CP01	12	f	left hemiplegic	1	crouch gait	normal	normal	normal
CP02	8	f	right hemiplegic	1	normal	equinus jump gait	high	high
CP03	13	f	right hemiplegic	1	normal	true equinus	normal	normal
CP04	12	m	spastic diplegia	2	crouch gait	crouch gait	high	high
CP05	20	m	spastic diplegia	2	apparent equinus	apparent equinus	normal	normal
CP06	5	f	spastic diplegia	2	equinus jump gait	equinus jump gait	high	high
CP07	11	m	diplegia	2	apparent equinus	apparent equinus	high	high
CP08	9	f	diplegia	2	crouch gait	crouch gait	high	high
CP09	10	m	right hemiplegic	2	normal	true equinus	normal	high
CP10	8	m	spastic diplegia	2	equinus jump gait	equinus jump gait	high	high
CP11	7	m	spastic diplegia	2	equinus jump gait	equinus jump gait	high	high
CP12	10	m	right hemiplegic	2	normal	true equinus	normal	low

[15,16,19,20]. The geometry was used to quantify the bending of the femoral shaft in sagittal and frontal plane. The previously developed and freely available GP-Tool (https://github.com/WilliKoller/GP-Tool) [20] was modified to create a hexahedral mesh with several layers of elements aligned with the proximal and distal growth plates based on the subject-specific femoral geometry. All operations were performed with software freely available for research purposes including Coreform Cubit, GIBBON [43] and MeshLab [44] and compiled MATLAB applications which can be run without a paying license. A subject-specific hexahedral mesh with an element size of approximately 1.5 mm was created for each femur (n = 50). For each participant, two representative steps (left and right) were chosen as loading condition. Similar to previous studies [16,19,20] nine load instances were selected based on the KCF peaks and the valley in-between during the stance phase. The medial and lateral KCF, PCF and muscle forces (n = 26) acting on the femur at these timepoints were used as loading conditions for FE analysis while nodes of the femoral head were constrained in all directions. Linear elastic materials were assigned to the different parts of the femur with varying Young's modulus and Poisson's ratio (Table S2). FEBio3 [45] was used for FE simulations and to calculate principal stresses in the distal growth plate.

2.3. Participant grouping

Limbs of participants with CP were grouped in three groups (CP_{normal}, $CP_{low\_knee\_flexion}$, $CP_{high\_knee\_flexion}$) depending on their knee flexion kinematics. Time-normalized knee flexion angles during the stance phase of each limb of CP participants was compared to the values obtained from the TD group. Knee flexion angle was considered as "low" or "high" if it was outside the mean ± 1.96 standard deviation range from the TD values for at least 5 % of the stance phase. If it was above and below the TD range at some time-points, the limb was included in the group where more time-points were outside the range.

2.4. Data analysis

Overall bone growth can be divided into the contribution of biological and mechanical factors [46]. Similar to previous studies, the growth rate due to mechanical loading was estimated as the osteogenic index (OI) [14–17,20,27,46]. The OI was calculated for each element in the growth plate using the obtained principal stresses from the FE analysis, details can be found in the Supplementary material. Positive and negative OI values indicate regions where growth is likely to be promoted or inhibited, respectively. Considering that bone mineralizes on the diaphyseal side, the OI was determined within the most proximal layer of the distal growth plate.

To enable a comparison of OI between growth plates with different shapes, the OI values were projected on a plane parallel to the growth plate and interpolated to a rectangle grid with a height to width ratio of 0.5. The rectangle was divided into four regions according to their corresponding anatomical sides of the growth plate separated by diagonals. A blue to red color scheme was used to visualize OI values revealing the OI distribution (anterior/posterior and medial/lateral) within each growth plate based on the mechanical loading condition (Fig. 1A). A representative OI distribution heatmap was created across limbs for each group.

Additionally, the region with the highest mean value was identified which indicates the area with maximally promoted growth. To assess the differences in OI between groups, we analyzed the mean occurring OI values in each region. The mean value of each region was normalized to the range of the individual OI and compared between groups. Furthermore, we evaluated the absolute range of the OI magnitude and the mean value of the OI. To quantify differences in shape and distribution, we compared each individuals OI heatmap with all OI heatmaps of TD participants with an image comparison method using OpenCV's template matching [47].

To identify possible reasons for observed differences of the OI between the TD and CP groups, the orientation between the distal growth plate and joint contact forces was evaluated. The angles between the normal vector of the growth plate identified with principal component analysis and the orientation of the medial and lateral KCF and PCF were calculated across the stance phase. Additionally, the orientation of the growth plate in the femoral coordinate system was evaluated (Fig. 1B).

2.5. Statistics

Significant differences between groups were quantified with ANOVAs. Statistical Parametric Mapping (SPM) [48] based on the SPM1D package (http://www.spm1d.org/) was used to compare time-dependent waveforms. In case of significance ($p < 0.05$), post-hoc tests with Bonferroni correction were used for pairwise comparisons.

3. Results

3.1. Participant groups and femoral bending

CP limbs were grouped depending on their knee flexion kinematics resulting in group sizes of 8, 1 and 15 for CP_{normal}, $CP_{low\_knee\_flexion}$ and $CP_{high\_knee\_flexion}$, respectively (Fig. 2A). SPM analysis revealed a significant different knee angle throughout the whole stance phase between TD and $CP_{high\_knee\_flexion}$ groups. No significant differences were observed when the TD group was compared to the CP_{normal} group. Due to the fact, that only one limb was part of the $CP_{low\_knee\_flexion}$ group, differences were not tested for significance and are not presented in the results of the main manuscript. All results and figures including this limb are available in the Supplementary material. Walking speed normalized

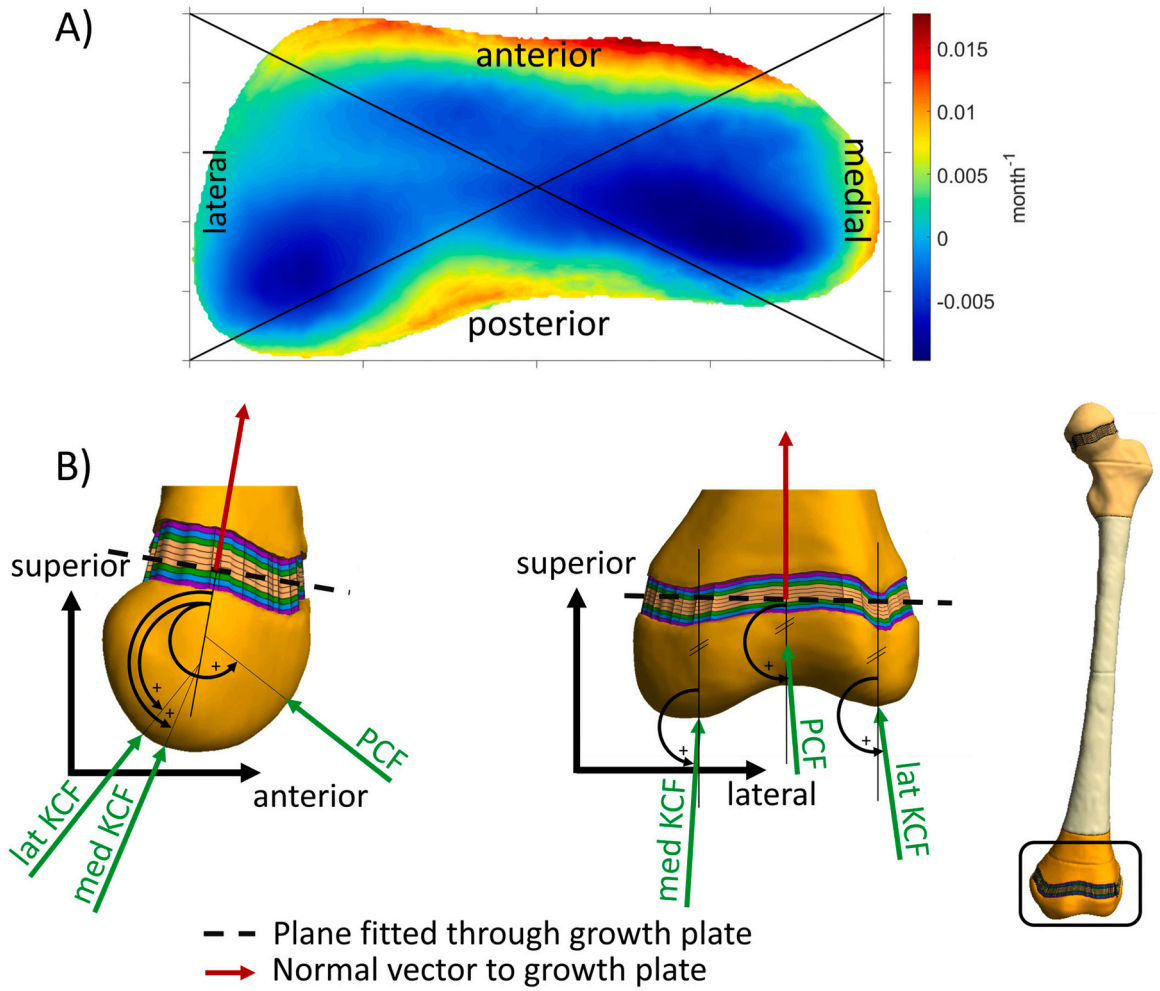

Fig. 1. A) An example of a projection of osteogenic index (OI) values on the plane parallel to the growth plate showing the division into four regions. The OI distribution is represented using a blue to red color scheme representing low and high values, respectively. B) Schematic illustration showing the orientation of the normal vector to the growth plate, medial and lateral knee joint contact force (KCF) and patellofemoral joint contact force (PCF) in sagittal and frontal plane and its corresponding angles.

to leg length [49] did not differ significantly between TD and $CP_{high\_knee\_flexion}$ group (Fig. 2C). Lower body kinematics of the groups are reported in the Supplementary material (Fig. S1). The anterior bending of the femoral shaft was significantly different between all groups in sagittal plane showing that participants of the TD group had the straightest femurs, followed by limbs of the CP_{normal} and $CP_{high\_knee\_flexion}$ group. In the frontal plane, limbs with high knee flexion had a higher lateral bending compared to the TD and CP_{normal} group (Fig. 2D).

3.2. Joint contact force and growth plate orientation

There were no significant differences in joint contact forces acting on the distal femur, i.e. medial and lateral KCF as well as PCF between the TD and CP_{normal} group. The $CP_{high\_knee\_flexion}$ group had significantly increased medial and lateral KCFs at the first peak and significantly higher PCF throughout the whole stance phase compared to the TD group (Fig. 3).

The orientation of the distal growth plate within the femur coordinate system showed no significant differences in the frontal and sagittal plane between all groups (Fig. 4A). In the frontal plane, medial and lateral KCF as well as PCF orientation showed no significant differences between groups (Fig. 4B–D) with values around 180° (approximately perpendicular to the growth plate). SPM revealed significant differences for the orientation of all three evaluated joint contact forces in the sagittal plane between the TD and $CP_{high\_knee\_flexion}$ group. More precisely, medial KCF was significantly different throughout 50 % of the stance phase, lateral KCF and PCF during the complete stance phase. The observed angles were lower, showing that the direction of the KCF points more anteriorly and the PCF points less posterior and more superior in respect to the growth plate orientation.

3.3. Osteogenic index reference dataset and differences between groups

The representative reference OI distribution heatmap generated from data of 26 TD limbs showed highest values in the posterior notch region and on the medial-anterior edge. The edges of the remaining growth plate have average values surrounding the middle where lowest OI values occurred. The OI distribution heatmap of eight limbs within the CP_{normal} group had its peak values in similar areas as the TD group but with additional peaks at the anterior-lateral edge. The OI distribution heatmap generated from data of 15 limbs of the $CP_{high\_knee\_flexion}$ group showed a linear gradient from high to low values from anterior to posterior side (Fig. 5A).

The highest mean value was observed in the posterior region in 88.5 % (n = 23) and 37.5 % (n = 3) of the limbs within the TD and CP_{normal} groups, respectively. The anterior region was the area with the highest mean value in 100 % (n = 15), 50 % (n = 4) and 11.5 % (n = 3) of the limbs of the $CP_{high\_knee\_flexion}$, CP_{normal} and of the TD group. In one

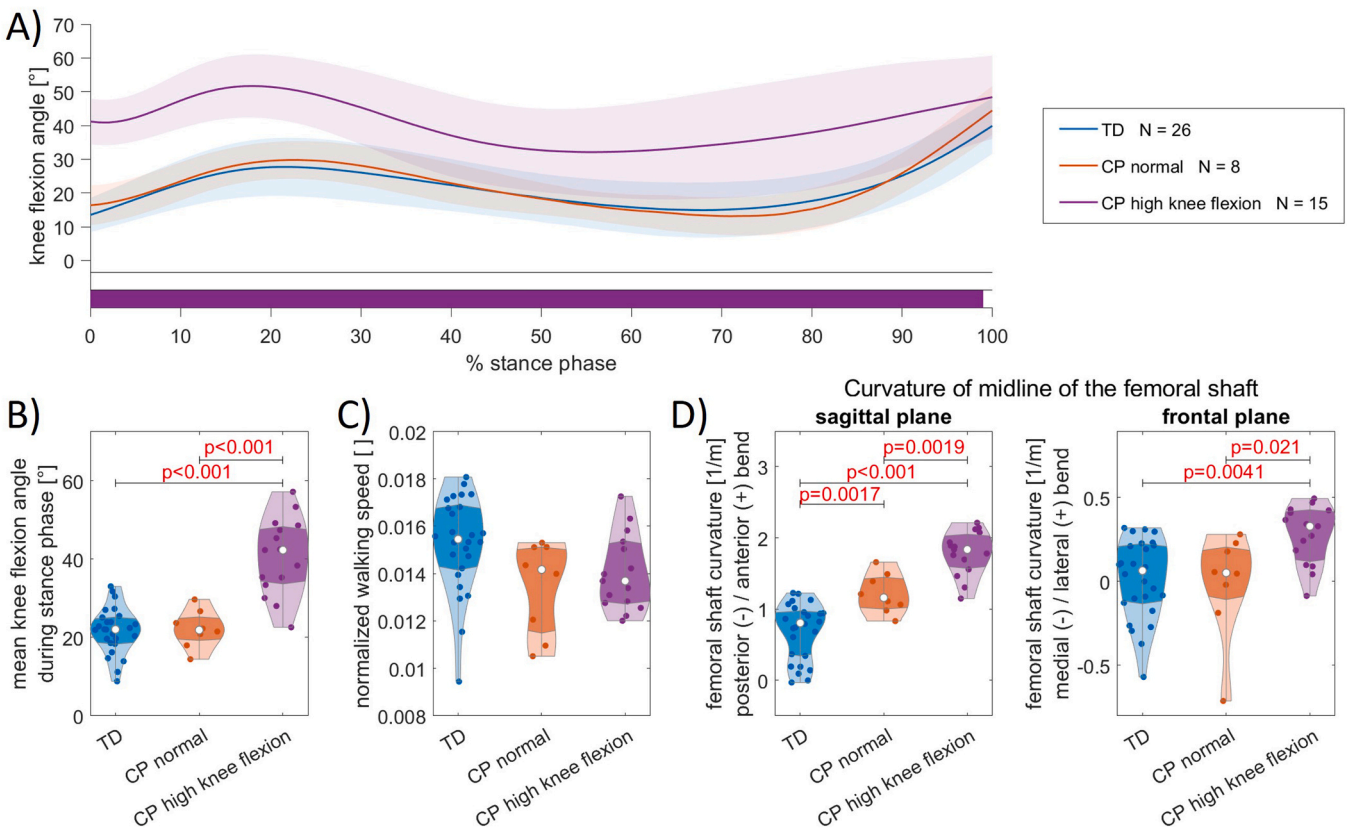

Fig. 2. A) Mean knee flexion angle and standard deviation (shaded) during the stance phase. Significant differences between TD and CP groups identified with SPM are visualized by corresponding colored bars (orange = "TD vs CP_{normal}"; violet = "TD vs $CP_{high\_knee\_flexion}$"). B) Violinplots show mean knee flexion angle during the stance phase. C) Violinplots show the non-dimensional walking speed normalized to leg length [49]. D) Curvature of the femoral shaft determined as the reciprocal radius of a circle fit to the midline of the femoral shaft [50].

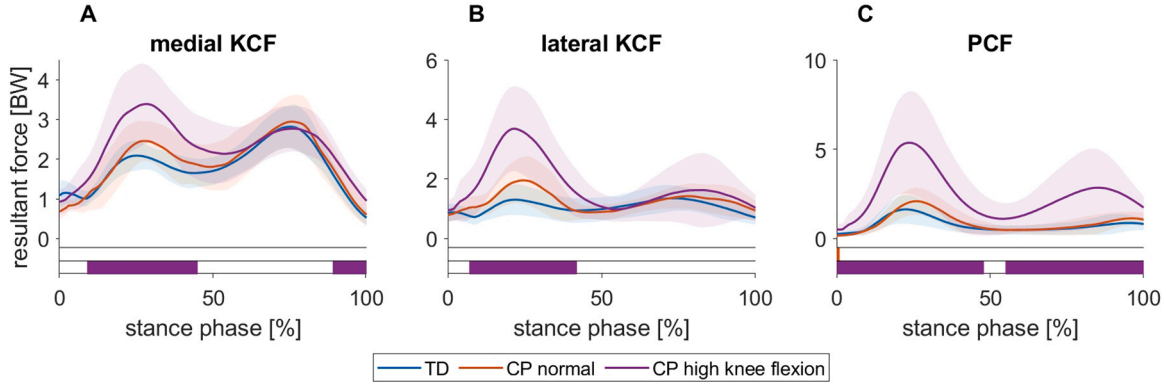

Fig. 3. Mean and standard deviation (shaded) of medial (A) and lateral KCF (B) and PCF (C) resulting magnitude during the stance phase. Significant differences between TD and CP groups identified with SPM are visualized by corresponding colored bars (orange = "TD vs CP_{normal}"; violet = "TD vs $CP_{high\_knee\_flexion}$") below each plot.

limb of the CP_{normal} group (12.5 %), the highest mean value was observed in the medial region (Fig. 5B left).

The mean values normalized to the range of the OI within medial and lateral regions showed no significant differences between the TD, CP_{normal} and $CP_{high\_knee\_flexion}$ groups. The normalized mean values within the posterior and anterior regions showed significant differences between each pairwise group comparison. Specifically, the OI magnitude in the posterior region was decreased in CP_{normal} and even more in $CP_{high\_knee\_flexion}$ groups whereas the mean values in the anterior region were increased in both groups compared to the TD group. (Fig. 5B right).

The range of the OI magnitude was significantly higher in the $CP_{high\_knee\_flexion}$ compared to the TD and CP_{normal} groups. CP_{normal} and $CP_{high\_knee\_flexion}$ groups had significantly lower mean OI values than the TD group. The image comparison to quantify differences in shape and distribution of the OI heatmaps revealed significant differences for each group comparison (Fig. 6).

4. Discussion

We analyzed stresses within the distal growth plate of the femur in a comparably large cohort of TD children and participants with CP. In agreement with our hypotheses we showed that the orientation of the

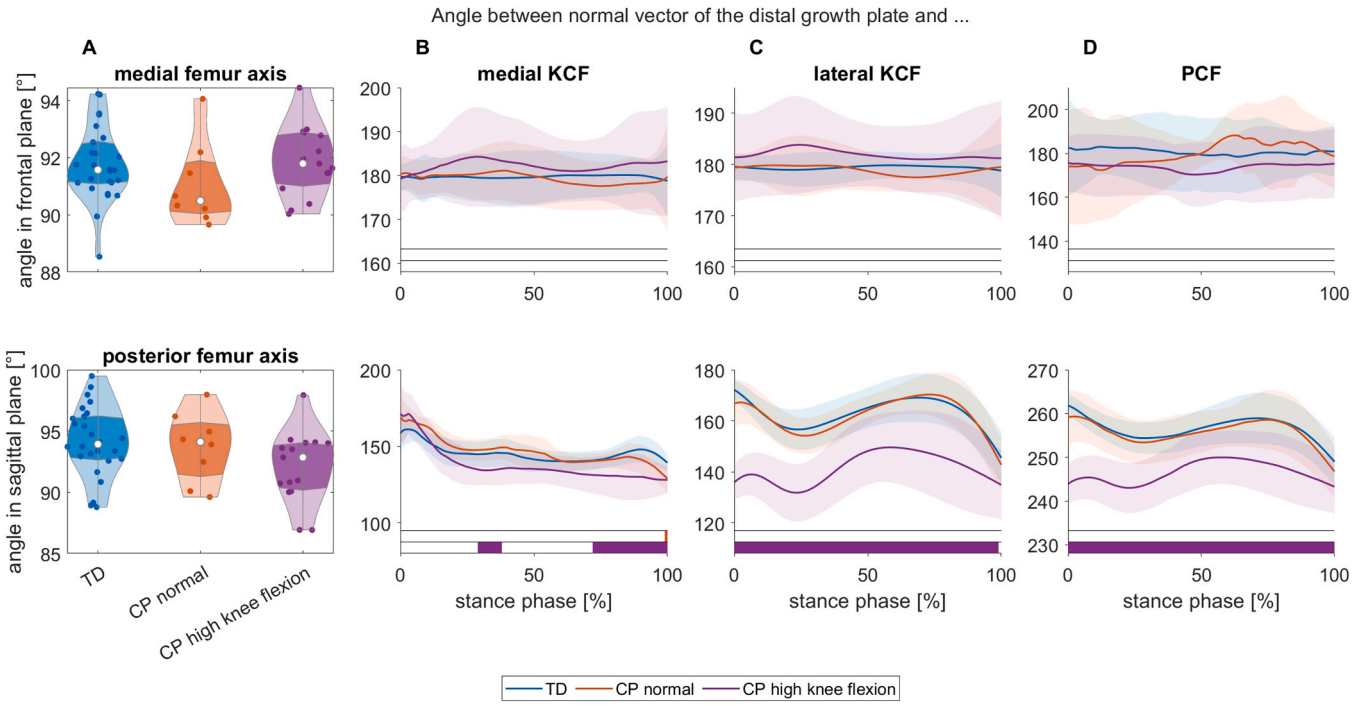

Fig. 4. A) Violinplots reveal the orientation of the distal growth plate in frontal and sagittal plane of the femur's coordinate system. B-D) Mean angle and standard deviation (shaded) between the normal vector of the distal growth plate and the medial (B) and lateral knee joint contact forces (KCF) (C) and patellofemoral joint contact force (PCF) (D) during the stance phase in the frontal and sagittal plane. Significant differences between TD and CP groups identified with SPM are visualized by corresponding colored bars (orange = "TD vs CP_{normal}"; violet = "TD vs $CP_{high\_knee\_flexion}$") below each plot. A schematic illustration on how the angles are expressed can be found in Fig. 1A.

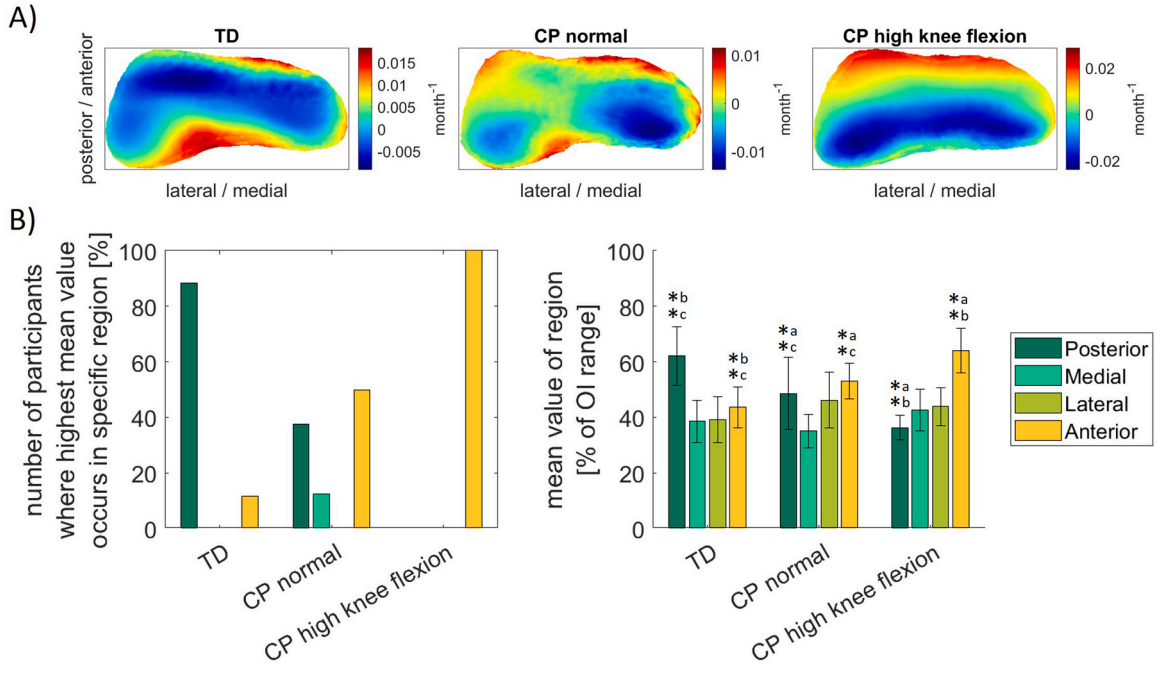

Fig. 5. A) Average distal growth plate shape and OI distribution in TD children, CP limbs with normal knee flexion and CP limbs with high knee flexion during stance phase. The OI distribution is represented using a blue to red color scheme representing low to high values, respectively. The unit is $months^{-1}$. B) The left plot shows how often the highest mean value was observed in a specific region. In the right plot the colored bars represent the mean value of each region normalized to the range of the individual OI. Vertical error bars indicate the standard deviation between limbs within groups. Significant differences were quantified with a two-way ANOVA with factors "region" and "group" where (*a) indicates significant differences to TD group, (*b) indicates significant differences to CP_{normal} group and (*c) indicates significant differences to the $CP_{high\_knee\_flexion}$ group.

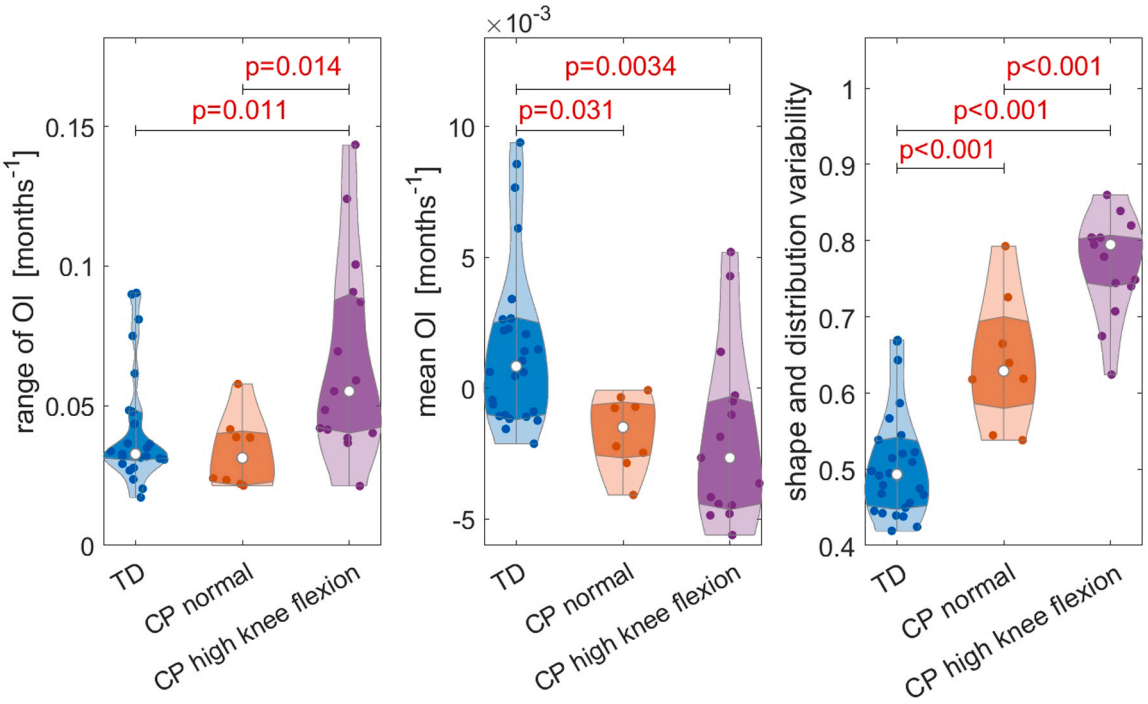

Fig. 6. Comparison of the variability of the magnitude of OI, i.e. range and mean value, and the variability assessed with template matching of the heatmaps. Each OI was compared to all OIs of the TD participants. Higher variability values indicate a higher difference in shape and distribution, a value of 0 indicates equality. Significant differences were quantified with ANOVAs with post-hoc Bonferroni correction for pairwise comparisons.

distal femoral growth plate is similar between TD and CP participants, but mechanical stress distribution differ between groups due to subject-specific gait patterns, muscle and joint contact forces.

As assumed, the growth plate orientation relative to the femoral coordinate system was similar in all groups. Additionally, or potentially consequently, the orientation of joint contact forces in respect to the growth plate was different in the $CP_{high\_knee\_flexion}$ group compared to the other groups. The more anteriorly oriented medial and lateral KCF promoted shear stresses while the more superiorly orientated PCF promoted compressive stresses within the growth plate in this group. This in combination with higher magnitudes of joint contact forces caused a higher range of OI values in the $CP_{high\_knee\_flexion}$ group, which could be interpreted as unevenly distributed growth.

CP limbs with typical knee flexion kinematics showed similar OIs within the distal growth plate as the TD group in terms of OI magnitude but a higher variability was revealed from image comparison of the OI heatmaps. These participants' kinematics showed a higher variability in frontal plane knee angle during the stance phase which could explain this finding. This means, CP participants with typical knee flexion kinematics during stance phase are likely to develop normal distal bone growth but the role of frontal plane knee kinematics should be further investigated as it might lead to different growth within medial and lateral regions of the distal growth plate. In this study, no significant differences regarding mean OI values in the medial and lateral regions, which could lead to potential varus/valgus malalignment, were found between groups.

Considering that high OI values indicate regions where bone growth and ossification is likely to occur, promoted growth in the anterior region compared to the posterior region would tilt the distal part of the femur posteriorly and, over a longer period, lead to higher anterior bending of the femoral shaft in the sagittal plane. This could potentially be a compensatory mechanism to normalize the angle between joint contact forces and the growth plate in the sagittal plane. In our participants, we found significantly higher femoral anterior bending in the sagittal plane in the $CP_{high\_knee\_flexion}$ compared to other groups which could be a result of progressive promoted growth in the anterior compartment. Patients with high anterior bend in the distal part of the femoral shaft, are not able to extend their leg completely as this would require a hyperextension at the knee. Hence, it cannot be said whether the knee flexion angle or the pre-existing high anterior bend is the cause, but our results indicate that both pathological patterns promote each other. To the best of the authors' knowledge, this is the first study to present OI values of the distal femoral growth plate, therefore, direct comparison to previous studies was not possible. Hucke et al. (2023) recently analyzed stresses within the distal femoral growth plate in three people with a pathological lower limb valgus alignment but did not use the OI for the presentation of their results. We provided the mean stress distribution of our groups in the same way as Hucke et al. [26] presented their results in the Supplementary material (Fig. S4). Differences in the estimated stresses in our study and Hucke et al. [26] are likely due to the different study cohort (healthy and CP participants versus children with pathological valgus alignment).We chose to analyze the OI since it is an established growth parameter, which has been used in several previous femoral growth studies and revealed physiological plausible results [17, 19,20]. OI distribution of the proximal growth plate of this cohort is presented in the Supplementary material. Furthermore, our simulations are in agreement with the observed increased curvature of the femur in the $CP_{high\_knee\_flexion}$ group compared to the other groups, as explained above.

It needs to be mentioned that, in addition to the high knee flexion angle during the stance phase, the $CP_{high\_knee\_flexion}$ group showed less external hip rotation and significantly higher internal rotation of the subtalar joint (Fig. S1). However, the increased knee flexion angle significantly altered the magnitude and orientation of KCFs as well as PCFs and therefore is likely to have a much bigger impact on growth plate stresses than the differences in transverse plane kinematics.

Age and sex are key factors for growth plate thickness which is relatable to potential remaining growth. The aim of this study was to enhance our understanding of the relationship between gait pattern, loading, growth plate geometry and orientation, and induced stresses. As we did not predict the bone growth but evaluated the stresses at a single time point, the thickness of the growth plate is not of importance

in our simulations. Therefore, one participant with closed epiphyseal plates was included in the study cohort to increase our sample size. In all participants, the geometry and orientation of the growth plate was clearly visible in the MRIs, even in the participant where the epiphyseal plate was already closed.

Our study included some limitations common for MSK simulations, i.e. generic muscle properties and motor control [51,52], and FE simulations, i.e. number of components included and material properties. Furthermore, we personalized tibia torsion only in a subset of our participants [53]. Each of these limitations and its possible effect on the results of this study is addressed in detail in the Supplementary material.

To conclude, this is the first study which evaluated stresses within the distal growth plate in a large cohort including different walking styles with subject-specific MSK models and bony geometry. Significant differences in OI were observed between TD participants and participants with CP. Our findings revealed that the knee flexion angle during the stance phase has a big impact on growth plate stresses at the distal femur. The simulation results of this study can serve as a reference dataset for future investigations. We would like to encourage peers to use the freely available GP-Tool (https://github.com/WilliKoller/GP-Tool) and conduct similar studies with large sample sizes to improve our general understanding of typical and pathological femoral bone growth with the ultimate goal to support and improve clinical decision making. If pathological femoral bone growth can be predicted at an early stage, subject-specific therapies like physiotherapy, orthosis or real-time biofeedback training could be used to alter joint loads [54–56] and therefore normalize growth plate stresses in the future.

Conflict of interest statement

The authors declare no conflict of interest.

Ethics approval was obtained from the local ethics committees (University of Vienna, reference no. 00578).

Funding

This research was partly funded by a PhD grant from the PhaNuSpo Vienna Doctoral School.

CRediT authorship contribution statement

Arnold Baca: Writing – review & editing, Supervision, Project administration, Funding acquisition, Conceptualization. **Hans Kainz:** Writing – review & editing, Visualization, Validation, Supervision, Methodology, Funding acquisition, Data curation, Conceptualization. **Willi Koller:** Writing – review & editing, Writing – original draft, Visualization, Validation, Methodology, Investigation, Formal analysis, Data curation, Conceptualization. **Jana Holder:** Writing – review & editing, Methodology. **Elias Wallnöfer:** Writing – review & editing, Visualization, Methodology. **Gabriel Mindler:** Writing – review & editing, Methodology. **Andreas Kranzl:** Writing – review & editing, Methodology, Data curation.

Declaration of Competing Interest

We wish to confirm that there are no known conflicts of interest associated with this publication and there has been no significant financial support for this work that could have influenced its outcome. We, further, confirm that the manuscript has been read and approved by all named authors and that there are no other persons who satisfied the criteria for authorship but are not listed.

Data Availability Statement

The code of the developed toolbox as well as an executable file is made freely available through a GitHub repository (https://github.com/WilliKoller/GP-Tool) including example data to perform the multi-scale workflow.

Appendix A. Supporting information

Supplementary data associated with this article can be found in the online version at doi:10.1016/j.gaitpost.2024.06.012.

References

[1] J.M. Rodda, H.K. Graham, G.R. Nattrass, M.P. Galea, R. Baker, R. Wolfe, Correction of severe crouch gait in patients with spastic diplegia with use of multilevel orthopaedic surgery, J. Bone Jt. Surg. 88 (2006) 2653–2664, https://doi.org/10.2106/JBJS.E.00993.

[2] A.M. Arkin, J.F. Katz, The effects of pressure on epiphyseal growth: the mechanism of plasticity of growing bone, JBJS 38 (1956) 1056–1076.

[3] R.T. Whalen, D.R. Carter, C.R. Steele, Influence of physical activity on the regulation of bone density, J. Biomech. 21 (1988) 825–837, https://doi.org/10.1016/0021-9290(88)90015-2.

[4] F. Rauch, Bone growth in length and width: the Yin and Yang of bone stability, J. Musculoskelet. Neuron Interact. 5 (2005) 194.

[5] D.R. Carter, G.S. Beaupré, Skeletal Function and Form: Mechanobiology of Skeletal Development, Aging, and Regeneration, Cambridge university press, 2007.

[6] T. Mirtz, The effects of physical activity on the epiphyseal growth plates: a review of the literature on normal physiology and clinical implications, J. Clin. Med. Res. (2011), https://doi.org/10.4021/jocmr477w.

[7] S.J. Mellon, K.E. Tanner, Bone and its adaptation to mechanical loading: a review, Int. Mater. Rev. 57 (2012) 235–255, https://doi.org/10.1179/1743280412Y.0000000008.

[8] G. Fabry, G.D. Macewen, A.R. Shands, Torsion of the femur: a follow-up study in normal and abnormal conditions, J. Bone Jt. Surg. 55 (1973) 1726–1738, https://doi.org/10.2106/00004623-197355080-00017.

[9] E.D. Bobroff, H.G. Chambers, D.J. Sartoris, M.P. Wyatt, D.H. Sutherland, Femoral anteversion and neck-shaft angle in children with cerebral palsy, Clin. Orthop. Relat. Res. 364 (1999) 194–204, https://doi.org/10.1097/00003086-199907000-00025.

[10] J. Robin, H.K. Graham, P. Selber, F. Dobson, K. Smith, R. Baker, Proximal femoral geometry in cerebral palsy: a population-based cross-sectional study, J. Bone Jt. Surg. Br. Vol. 90-B (2008) 1372–1379, https://doi.org/10.1302/0301-620X.90B10.20733.

[11] A.S. Arnold, A.V. Komallu, S.L. Delp, Internal rotation gait: a compensatory mechanism to restore abduction capacity decreased by bone deformity? Dev. Med. Child Neurol. 39 (2008) 40–44, https://doi.org/10.1111/j.1469-8749.1997.tb08202.x.

[12] H. Kainz, M. Wesseling, I. Jonkers, Generic scaled versus subject-specific models for the calculation of musculoskeletal loading in cerebral palsy gait: effect of personalized musculoskeletal geometry outweighs the effect of personalized neural control, Clin. Biomech. 87 (2021) 105402, https://doi.org/10.1016/j.clinbiomech.2021.105402.

[13] W. Koller, A. Baca, H. Kainz, The gait pattern and not the femoral morphology is the main contributor to asymmetric hip joint loading, PLoS One 18 (2023) e0291789, https://doi.org/10.1371/journal.pone.0291789.

[14] S.J. Shefelbine, D.R. Carter, Mechanobiological predictions of femoral anteversion in cerebral palsy, Ann. Biomed. Eng. 32 (2004) 297–305, https://doi.org/10.1023/B:ABME.0000012750.73170.ba.

[15] A. Carriero, I. Jonkers, S.J. Shefelbine, Mechanobiological prediction of proximal femoral deformities in children with cerebral palsy, Comput. Methods Biomech. Biomed. Eng. 14 (2011) 253–262, https://doi.org/10.1080/10255841003682505.

[16] P. Yadav, S.J. Shefelbine, E.M. Gutierrez-Farewik, Effect of growth plate geometry and growth direction on prediction of proximal femoral morphology, J. Biomech. 49 (2016) 1613–1619, https://doi.org/10.1016/j.jbiomech.2016.03.039.

[17] P. Yadav, S.J. Shefelbine, E. Pontén, E.M. Gutierrez-Farewik, Influence of muscle groups' activation on proximal femoral growth tendency, Biomech. Model. Mechanobiol. 16 (2017) 1869–1883, https://doi.org/10.1007/s10237-017-0925-3.

[18] P. Yadav, M.P. Fernández, E.M. Gutierrez-Farewik, Influence of loading direction due to physical activity on proximal femoral growth tendency, Med. Eng. Phys. (2021) S1350453321000217, https://doi.org/10.1016/j.medengphy.2021.02.008.

[19] H. Kainz, B.A. Killen, M. Wesseling, F. Perez-Boerema, L. Pitto, J.M. Garcia Aznar, S. Shefelbine, I. Jonkers, A multi-scale modelling framework combining musculoskeletal rigid-body simulations with adaptive finite element analyses, to evaluate the impact of femoral geometry on hip joint contact forces and femoral bone growth, PLoS One 15 (2020) e0235966, https://doi.org/10.1371/journal.pone.0235966.

[20] W. Koller, B. Gonçalves, A. Baca, H. Kainz, Intra- and inter-subject variability of femoral growth plate stresses in typically developing children and children with cerebral palsy, Front. Bioeng. Biotechnol. 11 (2023) 1140527, https://doi.org/10.3389/fbioe.2023.1140527.

[21] S.L. Delp, F.C. Anderson, A.S. Arnold, P. Loan, A. Habib, C.T. John, E. Guendelman, D.G. Thelen, OpenSim: open-source software to create and analyze dynamic simulations of movement, IEEE Trans. Biomed. Eng. 54 (2007) 1940–1950, https://doi.org/10.1109/TBME.2007.901024.

[22] K.M. Steele, M.S. DeMers, M.H. Schwartz, S.L. Delp, Compressive tibiofemoral force during crouch gait, Gait Posture 35 (2012) 556–560, https://doi.org/10.1016/j.gaitpost.2011.11.023.
[23] A. Seth, J.L. Hicks, T.K. Uchida, A. Habib, C.L. Dembia, J.J. Dunne, C.F. Ong, M. S. DeMers, A. Rajagopal, M. Millard, S.R. Hamner, E.M. Arnold, J.R. Yong, S. K. Lakshmikanth, M.A. Sherman, J.P. Ku, S.L. Delp, OpenSim: simulating musculoskeletal dynamics and neuromuscular control to study human and animal movement, PLoS Comput. Biol. 14 (2018) e1006223, https://doi.org/10.1371/journal.pcbi.1006223.
[24] Z.F. Lerner, M.S. DeMers, S.L. Delp, R.C. Browning, How tibiofemoral alignment and contact locations affect predictions of medial and lateral tibiofemoral contact forces, J. Biomech. 48 (2015) 644–650, https://doi.org/10.1016/j.jbiomech.2014.12.049.
[25] L. Modenese, M. Barzan, C.P. Carty, Dependency of lower limb joint reaction forces on femoral version, Gait Posture 88 (2021) 318–321, https://doi.org/10.1016/j.gaitpost.2021.06.014.
[26] L. Hucke, J. Holder, S. Van Drongelen, F. Stief, A.J. Gámez, A. Huß, A. Wittek, Influence of tension-band plates on the mechanical loading of the femoral growth plate during guided growth due to coronal plane deformities, Front. Bioeng. Biotechnol. 11 (2023) 1165963, https://doi.org/10.3389/fbioe.2023.1165963.
[27] H. Kainz, B.A. Killen, A. Van Campenhout, K. Desloovere, J.M. Garcia Aznar, S. Shefelbine, I. Jonkers, ESB clinical biomechanics award 2020: pelvis and hip movement strategies discriminate typical and pathological femoral growth – Insights gained from a multi-scale mechanobiological modelling framework, Clin. Biomech. 87 (2021) 105405, https://doi.org/10.1016/j.clinbiomech.2021.105405.
[28] G.M. Brouwer, A.W.V. Tol, A.P. Bergink, J.N. Belo, R.M.D. Bernsen, M. Reijman, H. A.P. Pols, S.M.A. Bierma-Zeinstra, Association between valgus and varus alignment and the development and progression of radiographic osteoarthritis of the knee, Arthritis Rheum. 56 (2007) 1204–1211, https://doi.org/10.1002/art.22515.
[29] J. Holder, Z. Feja, S. Van Drongelen, S. Adolf, H. Böhm, A. Meurer, F. Stief, Effect of guided growth intervention on static leg alignment and dynamic knee contact forces during gait, Gait Posture 78 (2020) 80–88, https://doi.org/10.1016/j.gaitpost.2020.03.012.
[30] P.M. Stevens, Guided growth for angular correction: a preliminary series using a tension band plate, J. Pediatr. Orthop. 27 (2007) 253–259, https://doi.org/10.1097/BPO.0b013e31803433a1.
[31] M. Gottliebsen, B. Møller-Madsen, H. Stødkilde-Jørgensen, O. Rahbek, Controlled longitudinal bone growth by temporary tension band plating: an experimental study, Bone Jt. J. 95-B (2013) 855–860, https://doi.org/10.1302/0301-620X.95B6.29327.
[32] M. Gottliebsen, J.M. Shiguetomi-Medina, O. Rahbek, B. Møller-Madsen, Guided growth: mechanism and reversibility of modulation, J. Child.'s Orthop. 10 (2016) 471–477, https://doi.org/10.1007/s11832-016-0778-9.
[33] H. Kainz, G.T. Mindler, A. Kranzl, Influence of femoral anteversion angle and neck-shaft angle on muscle forces and joint loading during walking, PLoS One 18 (2023) e0291458, https://doi.org/10.1371/journal.pone.0291458.
[34] E. Papageorgiou, A. Nieuwenhuys, I. Vandekerckhove, A. Van Campenhout, E. Ortibus, K. Desloovere, Systematic review on gait classifications in children with cerebral palsy: an update, Gait Posture 69 (2019) 209–223, https://doi.org/10.1016/j.gaitpost.2019.01.038.
[35] H. Kainz, H.X. Hoang, C. Stockton, R.R. Boyd, D.G. Lloyd, C.P. Carty, Accuracy and reliability of marker-based approaches to scale the pelvis, thigh, and shank segments in musculoskeletal models, J. Appl. Biomech. 33 (2017) 354–360, https://doi.org/10.1123/jab.2016-0282.
[36] L.H. Sloot, Advanced technologies to assess motor dysfunction in children with cerebral palsy, 2016.
[37] M. Sangeux, J. Pascoe, H.K. Graham, F. Ramanauskas, T. Cain, Three-dimensional measurement of femoral neck anteversion and neck shaft angle, J. Comput. Assist. Tomogr. 39 (2015) 83–85, https://doi.org/10.1097/RCT.0000000000000161.
[38] W. Yan, X. Xu, Q. Xu, W. Yan, Z. Sun, Q. Jiang, D. Shi, Femoral and tibial torsion measurements based on EOS imaging compared to 3D CT reconstruction measurements, Ann. Transl. Med. 7 (2019) 460, https://doi.org/10.21037/atm.2019.08.49.
[39] J.M. Kaneda, K.A. Seagers, S.D. Uhlrich, J.A. Kolesar, K.A. Thomas, S.L. Delp, Can static optimization detect changes in peak medial knee contact forces induced by gait modifications? J. Biomech. 152 (2023) 111569 https://doi.org/10.1016/j.jbiomech.2023.111569.
[40] A. Rajagopal, C.L. Dembia, M.S. DeMers, D.D. Delp, J.L. Hicks, S.L. Delp, Full-body musculoskeletal model for muscle-driven simulation of human gait, IEEE Trans. Biomed. Eng. 63 (2016) 2068–2079, https://doi.org/10.1109/TBME.2016.2586891.
[41] K. Veerkamp, H. Kainz, B.A. Killen, H. Jónasdóttir, M.M. van der Krogt, Torsion tool: an automated tool for personalising femoral and tibial geometries in OpenSim musculoskeletal models, J. Biomech. 125 (2021) 110589, https://doi.org/10.1016/j.jbiomech.2021.110589.
[42] A. Fedorov, R. Beichel, J. Kalpathy-Cramer, J. Finet, J.-C. Fillion-Robin, S. Pujol, C. Bauer, D. Jennings, F. Fennessy, M. Sonka, J. Buatti, S. Aylward, J.V. Miller, S. Pieper, R. Kikinis, 3D Slicer as an image computing platform for the Quantitative Imaging Network, Magn. Reson. Imaging 30 (2012) 1323–1341, https://doi.org/10.1016/j.mri.2012.05.001.
[43] K.M. Moerman, GIBBON: the geometry and image-based bioengineering add-on, JOSS 3 (2018) 506, https://doi.org/10.21105/joss.00506.
[44] P. Cignoni, M. Callieri, M. Corsini, M. Dellepiane, F. Ganovelli, G. Ranzuglia, MeshLab: an open-source mesh processing tool, in: V. Scarano, R.D. Chiara, U. Erra (Eds.), Eurographics Italian Chapter Conference, The Eurographics Association, 2008, https://doi.org/10.2312/LocalChapterEvents/ItalChap/ItalianChapConf2008/129-136.
[45] S.A. Maas, B.J. Ellis, G.A. Ateshian, J.A. Weiss, FEBio: finite elements for biomechanics, J. Biomech. Eng. 134 (2012) 011005, https://doi.org/10.1115/1.4005694.
[46] S.S. Stevens, G.S. Beaupré, D.R. Carter, Computer model of endochondral growth and ossification in long bones: biological and mechanobiological influences, J. Orthop. Res. 17 (1999) 646–653, https://doi.org/10.1002/jor.1100170505.
[47] G. Bradski, The OpenCV library, Dr. Dobb's J. Softw. Tools (2000).
[48] T.C. Pataky, M.A. Robinson, J. Vanrenterghem, Vector field statistical analysis of kinematic and force trajectories, J. Biomech. 46 (2013) 2394–2401, https://doi.org/10.1016/j.jbiomech.2013.07.031.
[49] A.L. Hof, Scaling gait data to body size, Gait Posture 4 (1996) 222–223, https://doi.org/10.1016/0966-6362(95)01057-2.
[50] V. Pratt, Direct least-squares fitting of algebraic surfaces, ACM SIGGRAPH Comput. Graph. 21 (1987) 145–152.
[51] B. Hanssen, N. Peeters, I. Vandekerckhove, N. De Beukelaer, L. Bar-On, G. Molenaers, A. Van Campenhout, M. Degelaen, C. Van den Broeck, P. Calders, K. Desloovere, The contribution of decreased muscle size to muscle weakness in children with spastic cerebral palsy, Front. Neurol. 12 (2021) 692582, https://doi.org/10.3389/fneur.2021.692582.
[52] N. Peeters, B. Hanssen, L. Bar-On, F. De Groote, N. De Beukelaer, M. Coremans, C. Van den Broeck, B. Dan, A. Van Campenhout, K. Desloovere, Associations between muscle morphology and spasticity in children with spastic cerebral palsy, Eur. J. Paediatr. Neurol. 44 (2023) 1–8, https://doi.org/10.1016/j.ejpn.2023.01.007.
[53] H. Kainz, A. Kranzl, In-toeing gait requires less muscular effort and reduces lower limb joint loads in people with internal torsional deformities, Gait Posture 97 (2022) S391–S392, https://doi.org/10.1016/j.gaitpost.2022.07.239.
[54] E. Comellas, S.J. Shefelbine, The role of computational models in mechanobiology of growing bone, Front. Bioeng. Biotechnol. 10 (2022) 973788, https://doi.org/10.3389/fbioe.2022.973788.
[55] S.D. Uhlrich, R.W. Jackson, A. Seth, J.A. Kolesar, S.L. Delp, Muscle coordination retraining inspired by musculoskeletal simulations reduces knee contact force, Sci. Rep. 12 (2022) 9842, https://doi.org/10.1038/s41598-022-13386-9.
[56] H. Kainz, W. Koller, E. Wallnöfer, T.R. Bader, G.T. Mindler, A. Kranzl, A framework based on subject-specific musculoskeletal models and Monte Carlo simulations to personalize muscle coordination retraining, Sci. Rep. 14 (2024) 3567, https://doi.org/10.1038/s41598-024-53857-9.